

A Nanostructure Phosphor: Effect of Process Parameters on the Photoluminescence Properties for Near-UV WLED Applications

H. Sameie · R. Salimi · A. A. Sabbagh Alvani · A. A. Sarabi ·
F. Moztarzadeh · M. A. Mokhtari Farsi · H. Eivaz Mohammadloo ·
M. Sabbagh Alvani · M. Tahriri

Received: 26 August 2011 / Accepted: 29 October 2011 / Published online: 11 November 2011
© Springer Science+Business Media, LLC 2011

Abstract The sol–gel preparative method was employed to synthesize $\text{SrZn}_2\text{Si}_2\text{O}_7:\text{Eu}$ nanostructure phosphors for white-light emitting diodes. The effects of calcination temperature and atmosphere as two important process parameters on the structural, morphological and optical properties were investigated using comprehensive characterization methods such as X-ray diffraction, scanning and transmission electron microscopy (SEM and TEM) and photoluminescence spectra. The obtained phosphors are efficiently excited from 340 to 400 nm, which matches the near UV emitting InGaN chip and emits strong band peaking at 481 nm due to $4f^65d^1(^2D) \rightarrow 4f^7(^8S_{7/2})$ transition of Eu^{2+} ions. In this europium-doped host lattice, a partial reduction of Eu^{3+} to Eu^{2+} at high temperature during the synthesis in air according to the charge compensation model is perceived. Furthermore, for this sample forbidden f–f transitions of Eu^{3+} are observed. Finally, using Scherrer's equation the crystallite size of the

optimum products with color coordination of $x = 0.176$, $y = 0.193$ is estimated at ~ 30 nm, which was consistent with TEM observations.

Keywords Nanostructures · Sol–gel · Photoluminescence · Rare-earths

1 Introduction

The white light emitting diodes (LEDs) have received much attention. They have been the subject of interest during the past decade owing to their advantages in conventional fluorescent and incandescent lamp; e.g., low energy consumption, compactness, long lifetime, high brightness and environmental protection [1–3]. Many phosphor converted methods have been developed for producing white LEDs. The most convenient way to generate white light from an LED is to use a blue LED chip and a yellow-emitting phosphor, which are usually made of cerium-doped yttrium aluminum garnet ($\text{YAG}:\text{Ce}^{3+}$). However, this type of white light has a low color rendering index because of lack of color in the red region [4]. The other approach, in which red/green/blue tricolor phosphors are excited by near UV LED chips (350–400 nm) to generate white light, has been suggested [5, 6]. In order to increase the efficiency of white LEDs, these phosphors should have strong absorption and excitation in the near UV, and then emit the desired light. As a UV LED can offer a higher efficient solid state light [7], more and more attention is being paid to the development of new phosphors that can be excited in the near-UV and increase the efficiency of white light emitting solid-state devices [8, 9]. In past several decades, researches have focused on the rare-earth (Re) ion-doped silicate-based phosphors [10–14]

H. Sameie and R. Salimi contributed equally to this work.

H. Sameie · R. Salimi · A. A. Sarabi · M. A. Mokhtari Farsi ·
H. Eivaz Mohammadloo
Faculty of Polymer Engineering and Color Tech, Amirkabir
University of Technology, 15875-4413, Tehran, Iran

H. Sameie · R. Salimi · A. A. Sabbagh Alvani (✉)
Color and Polymer Research Center (CPRC), Amirkabir
University of Technology, 15875-4413, Tehran, Iran
e-mail: sabbagh_alvani@aut.ac.ir

F. Moztarzadeh · M. Tahriri
Biomaterials Group, Faculty of Biomedical Engineering,
Amirkabir University of Technology, 15875-4413, Tehran, Iran

M. Sabbagh Alvani
Faculty of Materials Science and Engineering, University
of New South Wales, Sydney NSW 2052, Australia

as inorganic functional materials. Among them, the Eu ion-doped strontium silicate phosphors seem to have considerable potential for application in various optical devices [15–19]. The Eu^{3+} ion, which is intrinsically stable under ambient conditions, exhibits the line emission features due to the forbidden $f-f$ transitions (located from 550–750 nm), while divalent europium ion, which is sensitive to oxygen and therefore unstable in air, shows narrow-band and broad-band emissions due to its $f-f$ and $f-d$ transitions [20–23]. Since divalent Eu^{2+} ions exist under limited conditions, no Eu^{2+} ion-containing compound can be obtained as a natural product. Therefore, the starting europium compound in preparing luminescent materials is always trivalent; and, in general, the reduction of Eu^{3+} to Eu^{2+} in solids needs an annealing process in a reducing atmosphere such as H_2 , H_2/N_2 mixture or CO. Among the different methods of preparing precursors, the sol-gel technique offers several processing advantages, mainly due to purity, homogeneity, lower calcining temperature and modification of material properties by changing synthetic conditions [24, 25]. Moreover, the surface area of powders produced from the sol-gel technique is very high, and high surface-area phosphors have better thermal conductivity when they are excited with high-energy photons [26, 27], which are favorable for the lifetime of UV GaN-based white-LED. In this study, a series of Eu^{2+} -doped $\text{SrZn}_2\text{Si}_2\text{O}_7$ phosphors were synthesized by the sol-gel method to optimize emission under a variety of calcination temperatures. In addition, a detailed investigation of the effect of atmosphere on the colorimetry and photoluminescence properties was carried out.

2 Experimental Procedure

2.1 Powder Synthesis

A series of samples of $\text{SrZn}_2\text{Si}_2\text{O}_7:0.04\text{Eu}^{2+}$ were prepared by the sol-gel method and calcined at different temperatures in a weakly reductive atmosphere. First, stoichiometric amounts of $\text{Sr}(\text{NO}_3)_2$, $\text{Zn}(\text{NO}_3)_2 \cdot 6\text{H}_2\text{O}$ were dissolved in ethanol and water. Then $\text{Si}(\text{C}_2\text{H}_5\text{O})_4$ ($\text{SiO}_2, 28.4\%$) (TEOS) was added to the mixture with stirring condition for 30 min. Afterwards, a desired amount of europium nitrate [$\text{Eu}(\text{NO}_3)_3 \cdot 6\text{H}_2\text{O}$] was added to the precursor solution and the pH was adjusted ~ 3 . A white sol was obtained after stirring for 2 h. A semi-transparent viscous gel can be obtained by evaporating the solvent at 60 °C for 3 days. The resulting gel was dried at 120 °C for 48 h. Finally, the dried gel was calcined at 900, 1000, 1100 and 1200 °C for 1 h under a mildly reducing atmosphere (5% H_2 + 95% N_2) to reduce $\text{Eu}^{3+} \rightarrow \text{Eu}^{2+}$. To investigate the effect of the atmosphere, another sample was calcined at 1,100 °C for 1 h in air.

2.2 Powder Characterization

2.2.1 X-Ray Diffraction (XRD)

The product powders were analyzed with a Bruker AXS: D8 ADVANCE. This instrument operated with voltage and current settings of 40 kV and 30 mA, respectively, with $\text{Cu-K}\alpha$ radiation (1.5405 Å). For qualitative analysis, XRD diagrams were recorded in the interval $5^\circ \leq 2\theta \leq 70^\circ$ at scan speed of $2^\circ/\text{min}$.

2.2.2 Scanning Electron Microscopy (SEM)

The powders were coated with a thin layer of gold by sputtering (EMITECH K450X, England) and then the microstructure was observed by SEM (Stereoscan S 360 Cambridge) that operated at an acceleration voltage of 10 kV.

2.2.3 Transmission Electron Microscopy (TEM)

The morphology of powders was characterized by TEM (Hitachi H-800 electron microscope). Carbon-coated 200 mesh copper grids were dipped into a dilute suspension of the powders. The particles were deposited onto the support grids from a dilute suspension in acetone or ethanol.

2.2.4 Fluorescence Spectroscopy (FS)

The fluorescence excitation and emission spectra were acquired at right angles on a Perkin-Elmer LS-55 fluorescence spectrophotometer. These spectra were measured using original reacting mixtures at room temperature with a single monochromator. The instrument parameters affecting photoluminescence intensity are as follows; measurement type: wavelength scan, scan mode: excitation/emission, data mode: fluorescence, ex. slit: 5.0 nm, em. slit: 5.0 nm, PMT voltage: 950 V.

3 Results and Discussion

3.1 XRD Analysis

Figure 1 shows the XRD patterns of the samples after heat treatment at various temperatures ranging from 900 to 1,200 °C. The formation of the $\text{SrZn}_2\text{Si}_2\text{O}_7$ phase begins at 900 °C; and, the observed diffraction peaks of this phase become sharper and stronger with increasing calcinating temperature from 900 to 1,100 °C. This data indicate that the crystallinity of $\text{SrZn}_2\text{Si}_2\text{O}_7$ powders increases. Furthermore, when calcination temperature increases from 900 to 1,000 °C, the peaks related to the SrSiO_3 phase

disappear. Figure 1c clearly shows that the crystallization of the $\text{SrZn}_2\text{Si}_2\text{O}_7$ precursor is completed at 1,100 °C; and, the tetragonal structure for $\text{SrZn}_2\text{Si}_2\text{O}_7$ is formed at this temperature (JCPDS file number 10-0051). However, if the calcination temperature is too high (say 1,200 °C), phase purity decreases. The phase purity of phosphors greatly affects the luminous efficiency; i.e., phosphor particles with higher phase purity have higher luminous efficiency [28]. Therefore, it is expected that 1,100 °C is a better temperature for calcination.

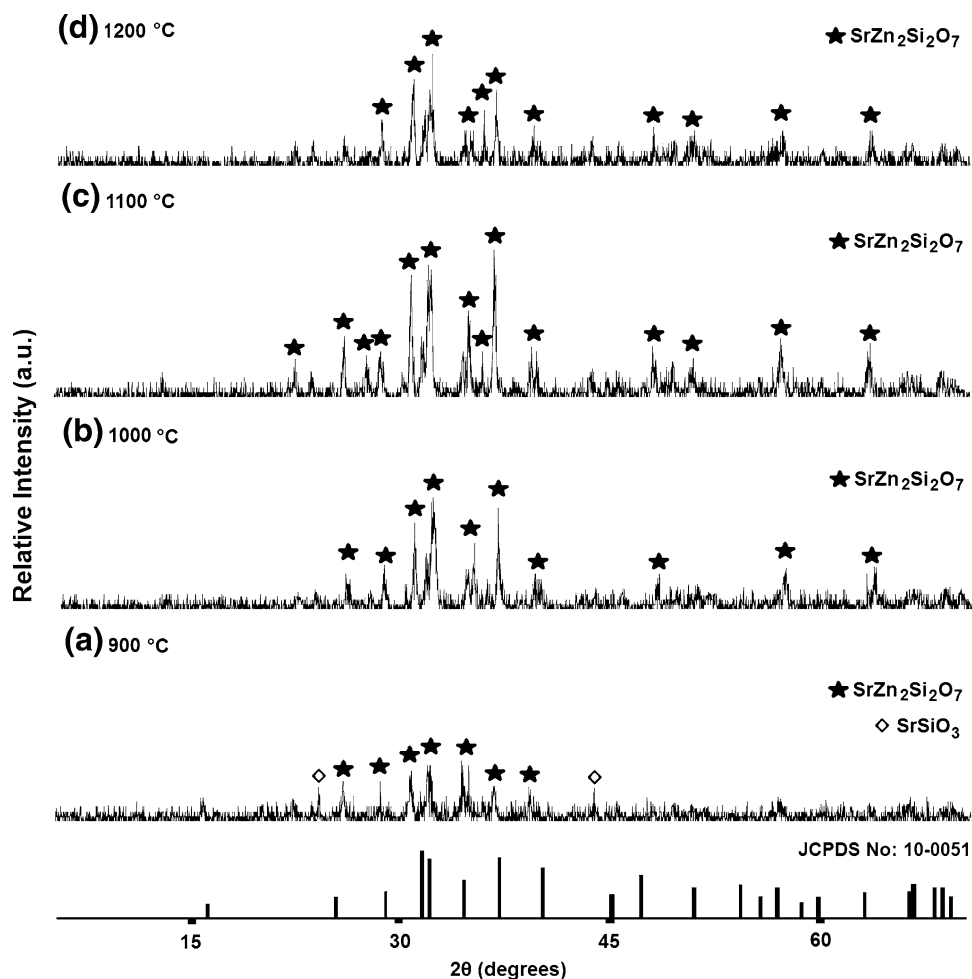
Figure 2a shows that the emission intensity of powders at near UV excitation is increased ~ 4 -fold on increasing the calcination temperatures from 900 to 1,100 °C. At lower temperatures, the decrease in emission intensities may be ascribed to the small amount of the Eu^{2+} ions that are diffused into the $\text{SrZn}_2\text{Si}_2\text{O}_7$ lattice [29]. With an increase in calcination temperatures, the Eu is distributed into the amorphous phase and diffuses into the $\text{SrZn}_2\text{Si}_2\text{O}_7$ lattice by rapid grain boundary diffusion; and, the emission intensities of the $\text{SrZn}_2\text{Si}_2\text{O}_7:\text{Eu}^{2+}$ powders are enhanced. In fact, the crystallinity and diffusion of dopants enhance by an increase in calcination temperature, which implies a decrease in the fluorescence quench centers (crystal

defects). Accordingly, the fall of non-radiative recombination leads to a luminescence intensity ascension. When the calcination temperature increased to 1,200 °C, the emission intensity decreased, which may be correlated to the destruction of the main phase and conglomeration of particles. The strong agglomeration is not profitable to the luminescence of a sample due to a decrease in the absorption of light [30]. The dopants have no obvious effect on the crystalline structure of the host. The Eu^{2+} ion, which acts as luminescent center in the $\text{SrZn}_2\text{Si}_2\text{O}_7$ host lattice, is expected to replace Sr^{2+} in the host. The ionic radius of Eu^{2+} and Sr^{2+} are close to a perfect match (viz. 1.25 and 1.26 Å, respectively) and substitution may finally give a new Eu(II) compound, which is iso-structural with the Sr^{2+} compound. The crystalline size was estimated from the broadening of the peaks using the Scherrer's formula,

$$D_{\text{hkl}} = k\lambda/\beta\cos\theta \quad (1)$$

where β is the width of the pure diffraction profile in radians, k is 0.89, λ the wavelength of the X-rays (0.15405 nm), θ the diffraction angle, and D_{hkl} is the average diameter of the crystallite. For this purpose, the

Fig. 1 XRD patterns of the $\text{SrZn}_2\text{Si}_2\text{O}_7$ gel heat treated at different temperatures



strongest diffraction Bragg peak is used to calculate the crystallite size. The results of these estimations are presented in Fig. 2b. Thus, the grain size of the phosphors is improved following the increase of the calcination temperature.

3.2 SEM and TEM Observations

SEM analysis was performed to study the morphology of the synthesized powders. Figure 3 illustrates SEM micrographs of the $\text{SrZn}_2\text{Si}_2\text{O}_7:\text{Eu}^{2+}$ phosphors obtained at various calcination temperatures. Clearly, the morphology converted from flower-like to nearly spherical-like shape

with increasing calcination temperature from 900 to 1,100 °C. Furthermore, as the calcining temperature was increased, the particle size became large. When the temperature was 1,100 °C (Fig. 3c), the particle size grew to $\sim 6 \mu\text{m}$ because of grain growth of larger grains by absorbing smaller grains. After heating at 1,200 °C, the densification process occurred and all the aggregates became much larger (Fig. 3d). Moreover, at high temperature, a sintering phenomenon occurred in some regions; and, the $\text{SrZn}_2\text{Si}_2\text{O}_7$ host crystals became surrounded by the molten grain boundary phase. Therefore, liquid phase sintering occurs when the calcination temperature is extensively high. The results indicate that increasing

Fig. 2 Emission spectra of $\text{SrZn}_2\text{Si}_2\text{O}_7:\text{Eu}^{2+}$ prepared at different temperatures (a) and dependence of emission intensity and grain size on calcination temperature (b)

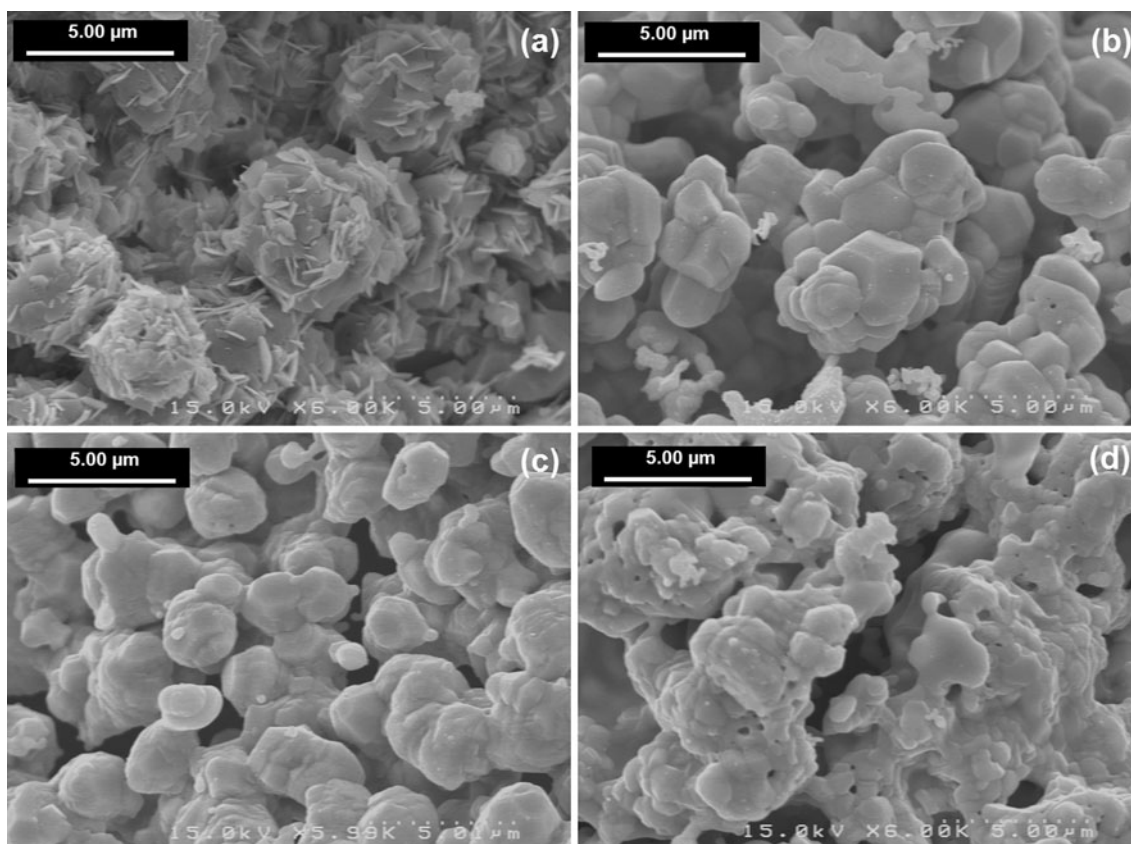
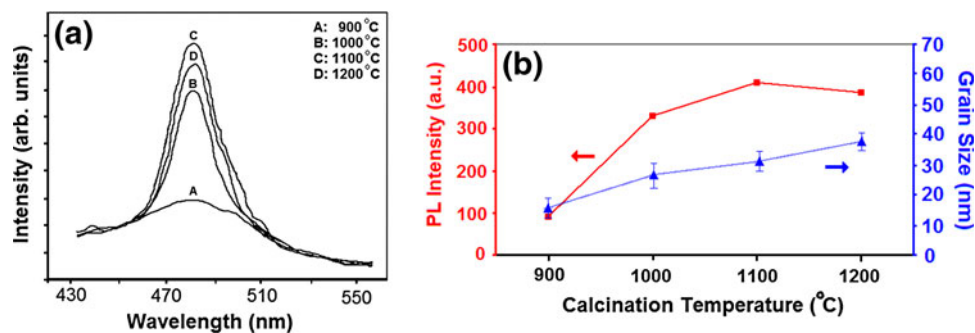


Fig. 3 SEM micrographs of $\text{SrZn}_2\text{Si}_2\text{O}_7:\text{Eu}^{2+}$ phosphor heated at 900 (a), 1000 (b), 1100 (c) and 1200 °C (d) for 1 h

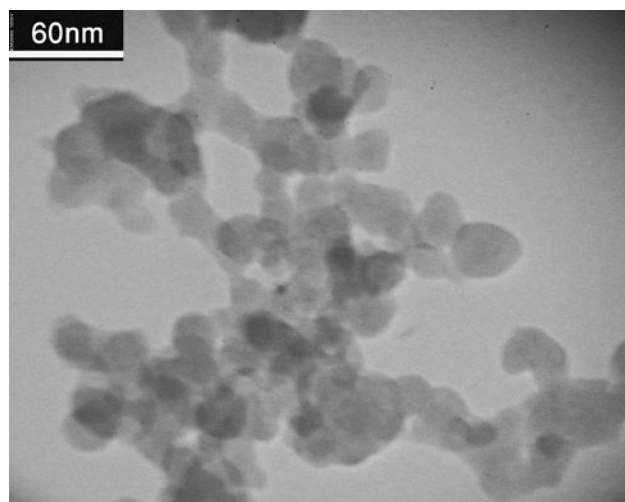


Fig. 4 TEM of the $\text{SrZn}_2\text{Si}_2\text{O}_7:\text{Eu}^{2+}$ phosphor prepared at 1,100 °C for 1 h

temperature effectively controls the product size and changes the shape of the particles.

Figure 4 shows the representative TEM micrograph for the $\text{SrZn}_2\text{Si}_2\text{O}_7:\text{Eu}^{2+}$ nanoparticles calcined at 1,100 °C. Here the particles have an approximately uniform size distribution and a spherical-like shape. Eventually, the size of the crystallites is $\sim 25\text{--}40$ nm, which is in agreement with the XRD data.

3.3 PL Properties

The PL excitation and emission spectra of $\text{SrZn}_2\text{Si}_2\text{O}_7:\text{Eu}$ synthesized in a weakly reductive atmosphere and air are presented in Fig. 5. When precursor is calcined in a reductive atmosphere, the main peak in the excitation spectrum is observed in 355 nm due to $5d\text{--}4f$ transition of Eu^{2+} . The strong and wide excitation spectrum at 335–395 nm and a conversion efficiency of 75% indicates that the phosphor is very suitable for a color converter using near-UV light as a primary light source. The material can be used as a blue phosphor excited by UV LED chip and mixed with other color emission phosphors to obtain white light. Moreover, the obtained phosphor from reductive atmosphere shows a

strong blue emission peaking at ~ 480 nm, which is attributed to a typical $4f^65d^1(^2D) \rightarrow 4f^7(^8S_{7/2})$ transition of Eu^{2+} . However, there is no special emission of Eu^{3+} for this sample, implying that Eu^{3+} ions have been completely reduced to Eu^{2+} in H_2 gas. Doubly- or triply-charged Eu ions can be present in ionic solids. For the case of the triply charged species, all $5d$ and $6s$ orbitals are empty and $4f$ is partially occupied. The optically active $4f$ electrons are shielded from the crystalline electric field by the outer $5s$ and $5p$ shells. The resulting effect is that the neighboring ligands have very little affection on the $4f$ electrons. For doubly-charged Eu ions, the energy separation between the $4f^7$ and $4f^65d^1$ configurations will be large and these transitions are dipole-allowed and are $\sim 10^6$ times more intense than the very frequently observed $4f \rightarrow 4f$ transitions in triply-charged Eu ions [31]. Therefore, a reducing atmosphere helps $\text{Eu}^{3+} \rightarrow \text{Eu}^{2+}$ ions to attain more blue emission intensity.

When the precursor is calcined in air, reduction of Eu^{3+} ions and $4f^65d^1(^2D) \rightarrow 4f^7(^8S_{7/2})$ transition of Eu^{2+} decreases. When the sample is prepared in air (Fig. 5b), emission peak at 481 nm decreases relative to the sample prepared in a reductive environment. Instead, emission lines from 570 to 620 nm, which clearly belonged to the $f\text{--}f$ transitions of Eu^{3+} ion, are observed (Fig. 5b(II)). The emission of Eu^{2+} ion in a solid state generally shows a broad band characteristic with a $4f^65d \rightarrow 4f^7$ transition, while Eu^{3+} ion always gives a series of typical emission lines in the from 570 to 750 nm, which corresponds to the $^5D_0\text{--}^7F_J$ ($J = 0,1,2,3,4$) transitions. This observation provides us a very convenient way to detect the presence of the Eu^{2+} ion in the solid state. The reduction phenomenon, $\text{Eu}^{3+} \rightarrow \text{Eu}^{2+}$, in $\text{SrZn}_2\text{Si}_2\text{O}_7:\text{Eu}$ prepared in air can be explained by the charge compensation model [32]. When trivalent Eu^{3+} ions are doped into the $\text{SrZn}_2\text{Si}_2\text{O}_7$, they replace the Sr^{2+} ions. To keep charge balance, two Eu^{3+} ions are needed to substitute for three Sr^{2+} ions (Fig. 6a). Hence, one vacancy defect, represented by two negative charges and two positive defects, are created by each substitution of every two Eu^{3+} ions in $\text{SrZn}_2\text{Si}_2\text{O}_7:\text{Eu}$. The Sr vacancy then acts as a donor of electrons, while the two Eu defects become acceptors of electrons. Consequently,

Fig. 5 Photoluminescence excitation (a) and emission (b) spectra of the $\text{SrZn}_2\text{Si}_2\text{O}_7:\text{Eu}$ synthesized in reductive atmosphere (I) and air (II)

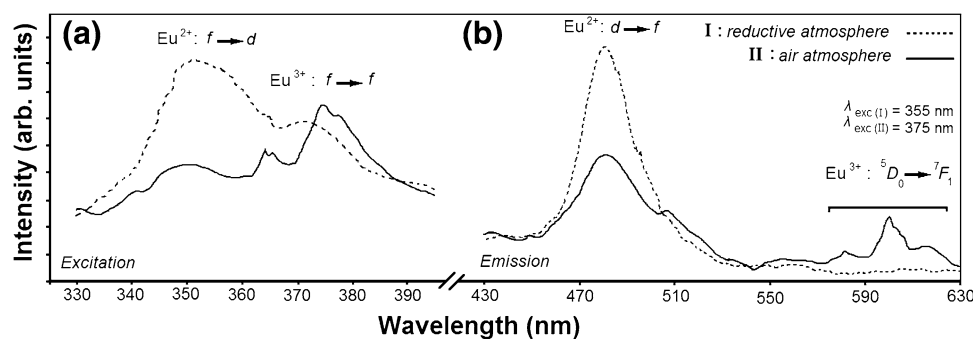
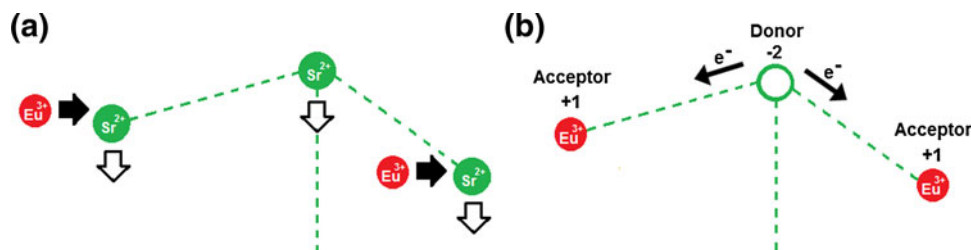


Fig. 6 The schematic graph of partial reduction of Eu^{3+} ions in the $\text{SrZn}_2\text{Si}_2\text{O}_7$ lattice



by thermal stimulation, the electrons in the vacancy defects of Sr are transferred to the Eu sites and partially reduce $\text{Eu}^{3+} \rightarrow \text{Eu}^{2+}$ (Fig. 6b). Hence, the reason for emission peaking at 480 nm for the sample prepared in air can be specified. Pie et al. [33] have systematically studied $\text{Eu}^{3+} \rightarrow \text{Eu}^{2+}$ the reduction process when the samples are prepared in air. They proposed a charge compensation model to explain the abnormal reduction. The basic requirements for a host lattice to affect the reduction of $\text{Eu}^{3+} \rightarrow \text{Eu}^{2+}$ in air at high temperature are the followings: (1) the doped rare earth ion should replace cations with lower valences in the host, such as alkaline earth ions; (2) no other reducible ions should be present in the host; (3) the radius of the cation that is substituted by Eu^{2+} should be similar to that of Eu^{2+} ; (4) the host compound should exhibit an appropriate crystal structure to stabilize the divalent rare earth ions at high temperature in a non-reducing atmosphere. The presently studied phases satisfy all the above criteria. Hence, a facile reduction of $\text{Eu}^{3+} \rightarrow \text{Eu}^{2+}$ could be affected by the synthesis of the phases in air.

3.4 Colorimetry

In general, color is represented by means of color coordinates. The chromaticity diagram established by the *International de l'Eclairage* (CIE) in 1931 is a two-dimensional graphical representation of any color perceivable by the human eye on an x - y plot. The evolution of colorimetric properties of two samples, which are calcined in a reductive atmosphere and air via this color space, is traced. Chromaticity coordinates of samples under short ultraviolet excitation are portrayed in Fig. 7. The diagram depicts that CIE coordinates of the samples are located in a blue region; but, the color purity of the sample prepared in air is lower than the phosphor produced in reductive atmosphere due to lower reduction possibility of the Eu ions.

Color coordinates and color temperature are two important characteristic for phosphors which may be used in light illuminants. The chromaticity coordinates for samples under D65 illustration are given in Table 1. According to the following approximate formula reported by McCamy [34], relative color temperatures of the samples may be also calculated by Eq. 2 (Table 1).

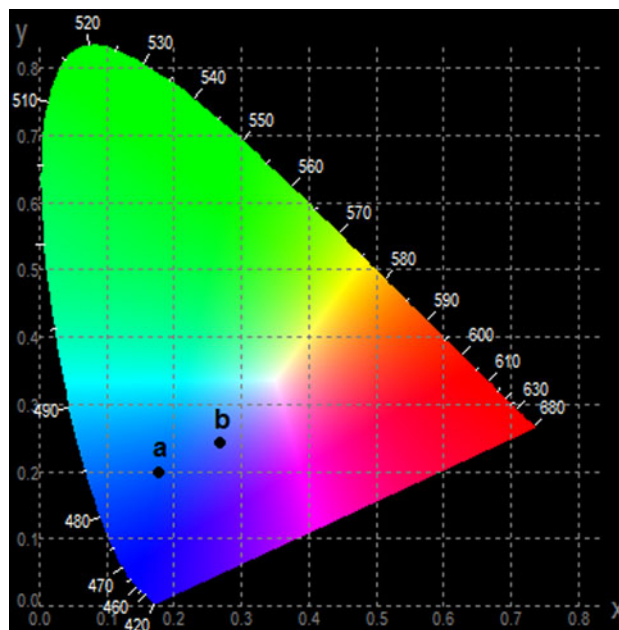


Fig. 7 x , y coordination by 1931-CIE standard chromaticity of the $\text{SrZn}_2\text{Si}_2\text{O}_7$:Eu phosphors synthesized in reductive atmosphere (a) and air (b)

Table 1 Comparison of CIE chromaticity coordinates of samples calcined reductive atmosphere (a) and air (b)

Sample	CIE chromaticity (x , y) coordinates	Color temperature (K)	Color purity (%)
a	(0.176, 0.193)	6783697.48	67
b	(0.269, 0.243)	180086.56	31
CIE illuminant D65	(0.313, 0.329)		

$$T = -437n^3 + 3601n^2 - 6861n + 5514.31 \quad (2)$$

where

$$n = (x - 0.332)/(y - 0.186)$$

4 Conclusions

The nanostructure blue-emitting phosphors are synthesized for near UV LED applications by wet-chemical route. The

emission intensities markedly increased with the calcination temperature up to 1,100 °C owing to an increase in the amount of the SrZn₂Si₂O₇ phase and diffusion of dopant ions into the host lattice. The calcination temperature converts morphological properties from flower-like to spherical shape. Under near UV excitation, Eu²⁺-activated SrZn₂Si₂O₇ samples show a strong blue emission centered at 481 nm due to 4f⁶5d¹(²D) → 4f⁷(⁸S_{7/2}) transitions of Eu²⁺. The reduction of Eu³⁺ → Eu²⁺ in air is observed in SrZn₂Si₂O₇:Eu phosphors prepared at high-temperature. The reason of this phenomenon is explained by a charge compensation model. The crystallite size of the optimum products with color purity of 67% is estimated at ~25–40 nm, which can be associated with the synthetic process (i.e., the sol–gel method).

Acknowledgments The authors would like to acknowledge Iran National Science Foundation (INSF) and Color & Polymer Research Center (CPRC) for helping us in this project.

References

1. A.H. Mueller, M.A. Petruska, M. Achermann, D.J. Werder, E.A. Akhador, D.D. Koleske, M.A. Hoffbauer, V.I. Kilmov, *Nano. Lett.* **5**, 1039 (2005)
2. F. Xiao, Y.N. Xue, Q.Y. Zhang, *Physica B* **404**, 3743 (2009)
3. Y.Q. Li, J.E.J. Van Steen, J.W.H. Van Kervel, G. Botty, A.C.A. Delsing, H.T. Hintzen, *J. Alloys Compd* **417**, 273 (2006)
4. S. Nakamura, G. Fasol, *The blue laser diode: GaN based blue light emitters and lasers* (Springer, Berlin, 1997), pp. 215–220
5. Y. Hu, W. Zhuang, H. Ye, S. Zhang, Y. Fang, X. Huang, *J. Lumin.* **111**, 139 (2005)
6. S.H.M. Poort, W. Janssen, G. Blasse, *J. Alloys Compd.* **260**, 93 (1997)
7. D.A. Steigerwald, J.C. Bhat, D. Collins, R.M. Fletcher, M.O. Holcomb, M.J. Ludowise, P.S. Martin, S.L. Rudaz, *IEEE J. Sel. Top Quantum Electron* **8**, 310 (2002)
8. M.G. Craford, N. Holonyak, F.A. Kish, *Sci. Am.* **284**, 62 (2001)
9. Z.L. Wang, H.B. Liang, M.L. Gong, Q. Su, *Electrochem Solid State Lett.* **8**, H33 (2005)
10. L. Zhang, X.M. Zhou, H.H. Zeng, H.Q. Chen, X.P. Dong, *Mater. Lett.* **62**, 2539 (2008)
11. A.A. Sabbagh Alvani, F. Moztarzadeh, A.A. Sarabi, *J. Lumin.* **115**, 147 (2005)
12. Y.C. Kang, H.D. Park, *Appl. Phys. Mater. Sci.* **77**, 529 (2003)
13. W.J. Park, Y.H. Song, D.H. Yoon, *Mater. Sci. Eng. B* **173**, 76 (2010)
14. B. Wang, L. Sun, H. Ju, *Solid State Commun.* **150**, 1460 (2010)
15. N. Lakshminarasimhan, U.V. Varadaraju, *Mater. Res. Bull.* **43**, 2946 (2008)
16. S.M. Levshov, I.V. Berezovskaya, N.P. Efrushina, B.I. Zadneprovskii, V.P. Dotsenko, *Inorg. Mater.* **47**, 285 (2011)
17. J.H. Lee, Y.J. Kim, *Mater. Sci. Eng. B* **146**, 99 (2008)
18. H. Sameie, R. Salimi, A.A. SabbaghAlvani, A.A. Sarabi, F. Moztarzadeh, M. Tahriri, *Physica B* **405**, 4796 (2010)
19. P.L. Li, Z.P. Yang, Z.J. Wang, Q.L. Guo, X. Li, *Chin. Sci. Bull.* **53**, 974 (2008)
20. S. Ye, F. Xiao, Y.X. Pan, Y.Y. Ma, Q.Y. Zhang, *Mater. Sci. Eng. R* **71**, 1 (2010)
21. R. Stefani, A.D. Maia, E.E.S. Teotonio, M.A.F. Monteiro, M.C.F.C. Felinto, H.F. Brito, *J. Solid State Chem.* **179**, 1086 (2006)
22. J.K. Han, G.A. Hirata, J.B. Talbot, J. McKittrick, *Mater. Sci. Eng. B* **176**, 436 (2011)
23. B. Liu, Y. Wang, J. Zhou, F. Zhang, Z. Wang, *J. Appl. Phys.* **106**, 053102 (2009)
24. A.M.M. Sautos, W.L. Vasconcelos, *J. Non-Cryst. Solids* **273**, 145 (2000)
25. J. Lin, K. Baerner, *Mater. Lett.* **46**, 86 (2000)
26. M. Pang, X. Liu, J. Lin, *J. Mater. Res.* **20**, 2676 (2005)
27. P. Yang, M.K. Lu, C.F. Song, D. Xu, D.R. Yuan, G.M. Xia, Y. Xi, S.W. Liu, J.X. Shen, *Mater. Res. Bull.* **38**, 757 (2003)
28. K.Y. Jung, H.W. Lee, Y.C. Kang, S.B. Park, Y.S. Yang, *Chem. Mater.* **17**, 2729 (2005)
29. P. Huang, C. Cui, S. Wang, *Opt. Mater.* **32**, 184 (2009)
30. U.S. Sias, E.C. Moreira, E. Ribeiro, *Nucl. Instrum. Methods B* **218**, 405 (2004)
31. G. Blasse, B.C. Grabmaier, *Luminescent materials* (Springer-Verlag, Berlin, 1994), pp. 25–28
32. M. Peng, Z. Pei, G. Hong, Q. Su, *Phys. Chem. Lett.* **371**, 1 (2003)
33. Z. Pei, Q. Zeng, Q. Su, *J. Solid State Chem.* **145**, 212 (1999)
34. C.S. McCamy, *Color Res. Appl.* **17**, 142 (1992)